PERFORMANCES OF A HGCDTE APD BASED DETECTOR WITH ELECTRIC COOLING FOR 2-μm DIAL/IPDA APPLICATIONS

A. Dumas[1]*, J. Rothman[2], F. Gibert[1], G. Lasfargues[2], J-P. Zanatta[2] and D. Edouart[1].

[1] ***LMD, École Polytechnique/CNRS, France, *Email: arnaud.dumas@lmd.polytechnique.edu***

[2] ***LETI, CEA - Campus Minatech, France***

1. ABSTRACT

In this work we report on design and testing of an HgCdTe Avalanche Photodiode (APD) detector assembly for lidar applications in the Short Wavelength Infrared Region (SWIR : 1,5 - 2 μm). This detector consists in a set of diodes set in parallel -making a 200 μm large sensitive area- and connected to a custom high gain TransImpedance Amplifier (TIA). A commercial four stages Peltier cooler is used to reach an operating temperature of 185K. Crucial performances for lidar use are investigated : linearity, dynamic range, spatial homogeneity, noise and resistance to intense illumination.

2. INTRODUCTION

Within the framework of greenhouse gases (GHG) monitoring with lidar, the Laboratoire de Météorologie Dynamique (LMD, IPSL, Paris) has developed a 2μm instrument dedicated to Differential Absorption Lidar (DIAL) and Integrated Path Differential Absorption (IPDA) techniques. Results on the laser emitter were reported in [1] and first CO_2 DIAL measurements using coherent detection are to be published. The main reason for using coherent detection at the time was the lack of a very highly-sensitive detector in SWIR. However, recent advances in the field of HgCdTe APD may have shifted the balance of power between direct and coherent detection.

Indeed, the remarkable properties for amplification of HgCdTe APD (large gain, low dark current and close to unity excess noise factor) makes this technology especially suitable for very low intensity signal detection in SWIR : on the one hand photomultiplier tube technology is not available because the energy per photon is not large enough to use external photoeffect [2], on the other hand, InGaAs APD have intrinsic limitation when it comes to amplification because of higher dark current and large excess noise factor. Today HgCdTe APD technology has reached some level of maturity and applications are currently investigated : space laser-based telecommunications, spectroscopy, lidar, etc.

The challenging issue for lidar use is to reach sufficiently large sensitive area while keeping a low level of noise. One proposal has been carried out at NASA Goddard Space Flight Center (GSFC) in collaboration with DRS technologies to develop a multi-element HgCdTe APD detector. This latter consists in an array of 16 independant pixels whose individual size is 80 μm. Each pixel is a set of four diodes set in parallel that inherit the p around n junction architecture. A Noise Equivalent Power (NEP) as low as 4 fW/$\sqrt{\text{Hz}}$ is reported when operated at 77K [3]. On the other hand, we have developed a single element detector from existing Focal Plane Array (FPA) matrix by connecting 37 diodes in parallel. This detector was manufactured at the Centre à l'Energie Atomique -Laboratoire d'Electronique et Techniques de l'Information (CEA-LETI) in Grenoble (France) and therefore inherits planar architecture for diode junctions. Regarding cooling, we made the decision to use Thermo-Electric Cooling (TEC) because it requires less energy, which is an appreciable asset for any space equipment.

In this study we first describe this detector design. Previous communication with wider scope on the development of this technology at CEA-LETI can be found here [4]. Then we report on test results for the detector figures of merit that are especially relevant for lidar use. Namely : dark current, spatial homogeneity, linearity, gain, NEP and resistance to intense illumination.

3. DESIGN OF LIDAR DETECTOR

A. Assembly overview

A side view of the detector assembly is presented in figure 1. The APD and the TIA are set up side by side within a cryostat. Distance between the APD and the TIA PCB is minimized to avoid parasite capacitance.

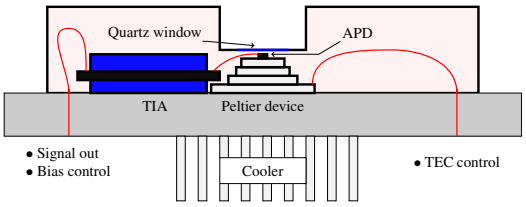

Figure 1: Sideview of the detector assembly that was developed at CEA-LETI.

A quartz window is used to enable IR illumination of the APD. This latter was set up as close to the APD as possible in order to use short focal lenses outside the cryostat. Commercial references and main characteristics of the commercial Peltier device and TIA are provided in table 1.

Table 1: References and characteristics for Peltier device and TIA.

Petier device :	TEC Marlow NL4040 ΔT = 120K
TIA :	FirstLightImaging Gain : 6,97·10^5 V/A (1% accuracy) Bandwidth : 20,5 MHz Input noise current density : 0,9 pA/$\sqrt{\text{Hz}}$

B. Requirements

For the setup presented in last section, the Noise Equivalent Power (NEP_W) in Watts can be expressed as [2]:

$$\frac{1}{M}\cdot\sqrt{<i^2_{\text{input TIA}}>_T+2q(i_d+i_s)M^2F\cdot\frac{1}{2T}}\cdot\frac{1}{\eta}\cdot\frac{hc}{q\lambda} \quad (1)$$

where M is the APD gain, $<i^2_{\text{input TIA}}>_T$ the variance of the input TIA current over a time interval with duration T, q the elementary charge, i_d the mean value of the dark current, i_s the mean value of the current converted photon signal, T the caracteristic time (defined as $1/2B$, where B is the bandwidth of the TIA), F the excess noise factor, h the Planck constant, c the speed of light and λ the wavelength.

As the NEP_W is often normalized per unit $\sqrt{\text{Hz}}$, we rewrite it NEP in W/$\sqrt{\text{Hz}}$ as follows :

$$\text{NEP}=\frac{1}{M}\sqrt{i^2_{TIA}+2q(i_d+i_s)M^2F}\cdot\frac{hc}{q\lambda}\cdot\frac{1}{\eta} \quad (2)$$

where i_{TIA} is the noise density at the input of the TIA (in A/$\sqrt{Hz}$). As long as the noise due to the TIA is dominant over the shot noise of the signal and the dark current, it is worth to increase the gain. Once the amplified shot noise or the amplified dark current dominates, any increase of the gain would decrease the signal to noise ratio because of the excess noise factor (see [2]). In particular, equation 2 shows that for a certain gain, a balance is obtained between dark current, shot noise amplification and TIA noise reduction.

A numerical model of APD gain as a function of reverse bias was used to compute the expectable gain at the temperature of 185K . The maximum value for reverse bias is limited to approximately 14V. Beyond this value, tunnel current is not negligible anymore. At 12 V reverse bias and 185 K temperature, a gain of approximately 40 is expected. For a NEP of 50 fW/$\sqrt{\text{Hz}}$ for instance, this means that the input referred current noise of the TIA should be lower than 2 pA/$\sqrt{\text{Hz}}$.

C. Macro-diode geometry

Usually in lidar applications, the telescope collecting mirror, which serves as pupil, is imaged onto the sensitive area of the detector. Indeed in such a configuration, the enlightened area of the detector is always the same, which is suitable to avoid potential errors due to spatial inhomogeneities of detector response. On the one hand, the larger the sensitive area, the easier it is to make the image of the pupil on it. On the other hand, a large sensitive area limits the performances of the diode itself, especially in terms of noise. As a result, the size of 200 μm stands as a trade off between these constraints.

The architecture of the macro photodiode is inherited from standard production of FPAs at CEA-LETI (see figure 2).

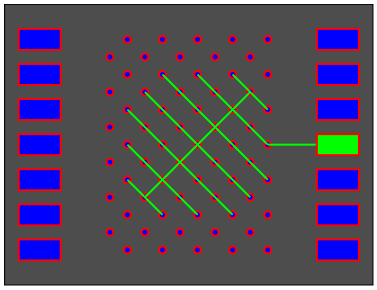

Figure 2: The macro APD structure is inherited from FPA production. 37 diodes are connected in parallel. Horizontal step between two diodes is roughly 40 μm.

Planar architecture is used and the 37 diodes are bonded in parallel on the front side. As a consequence, and because the detector is in this case back-side illuminated, remarkable homogeneity in photons collection is achieved (see experimental evaluation).

4. HGCDTE APD TEST RESULTS

Having presented the detector setup, we focus here on experimental tests that have been carried out to assess the macro-diode performances : dark current, spatial homogeneity of the response and response to intense flux. In these experiments the macro diode was isolated from the TIA described above and cooled with liquid nitrogen. This also means that the cryostat was different. Experimental conditions are described for each subsection.

A. Dark current

First the dark current has been evaluated to roughly 0.2 nA at 185 K(see figure 3). A cryostat with cold shield was used.

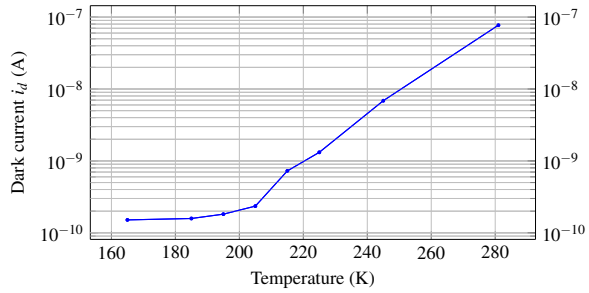

Figure 3: Dark current as a function of APD temperature

It should be noted that the observed current would rather be called residual current. Indeed as any object at ambient temperature emits in the SWIR region and despite of cold shield, some undesirable photons are always collected. Therefore the distinction between residual photonic noise and dark current is hard to grasp.

B. Spatial homogeneity

A so-called spotscan experiment has been performed to assess spatial response of the APD. A SWIR source is used together with a pupil and a imaging lens to form a 10 μm large spot. This spot can be moved to every position in a square of roughly 220 μm edge by use of commanded mirrors. In our configuration the APD was cooled to 77 K with liquid nitrogen and connected to a high-gain transimpedance amplifier. Let (x, y) be the coordinates of the spot within the square. For any (x, y) the intensity at the output of the APD is recorded and we obtain that way the APD spatial response.

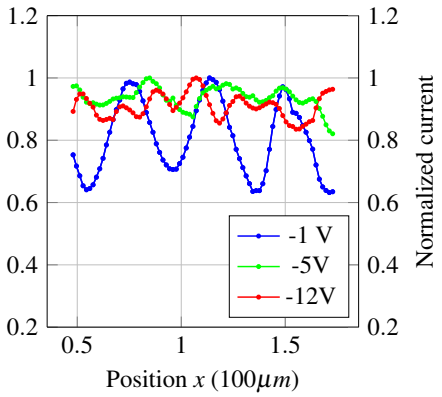

Figure 4: Relative variation of the normalized current along the central row for different reverse bias

One should be aware that the intensity figure obtained is the product of an optical intensity transfer function $\mathcal{H}(x, y)$ by the detector spatial response $\mathcal{R}(x, y)$. $\mathcal{H}$ accounts for any disturbing effect that modify the spot intensity at the position (x, y). It can be due to inhomogeneity of the source itself or to dust on optics for example. In the following paragraph we describe how we have managed to obtain an estimation of relative variation of $\mathcal{R}$.

We introduce $(\mathcal{G}_i)$ as the set of figures produced with a series of spotscan experiments during which the detector is steadily translated with respect to the square mentioned before. Namely, for any i, we have

$$\mathcal{G}_i(x, y) = \mathcal{R}(x + i\delta x, y)\mathcal{H}(x, y) \tag{3}$$

Therefore we can write

$$[\mathcal{G}_i(x, y)]_{i\in[n,m]} = \frac{\mathcal{H}(x, y)}{\mathcal{H}(x + \delta x, y)} \cdot [\mathcal{G}_i(x + \delta x, y)]_{i\in[n-1,m-1]} \tag{4}$$

From this set of measurements it is not possible to derive an absolute value of $\mathcal{R}$ but it is possible to express the relative difference of pixels along a row. From equation 4 we get relative variation of $\mathcal{H}$ along a row, and then variation of $\mathcal{R}$ along the x axis for different reverse bias. Figure 4 presents the results of this analysis. For 1 V reverse bias, the depletion area is not extended enough to collect efficiently photons that are incident far from the diode center. On the other hand, for reverse bias greater than 5 V, collection of photons is almost homogeneous. Slight heterogeneity of spatial response comes from manufacturing choices and flaws in experimental procedure. For a reverse bias of 5V, a standard deviation of 3.5 % for the set $\mathcal{R}(\cdot, y)$ where y corresponds to the central row of the APD. At a reverse bias of 12V, standard deviation is 3.8 %.

C. Behaviour under intense illumination

Previous experiences with space lidar have shown that because of intense reflexion on clouds, the detector might be intensely illuminated by such an echo. We have reproduced these conditions in order to estimate a damage threshold in terms of power as well as a recovery time. Therefore incident optical power was gradually increased as well as reverse bias. We went up to 20V reverse bias and 10 μW incident average power without noticing any damage. Depolarization of the diode was observed as a result of the mitigation voltage induced by the current in the series resistance.

5. DETECTOR ASSEMBLY TEST RESULTS

The results presented in this section concern the detector assembly, ie the APD with thermo-electric cooling and the TIA presented in first section. Therefore they account for the global behaviour of the macro APD plus the TIA.

A. Thermo-electric cooling efficiency

For ambient temperature of approximately 23 degrees and a pressure inside the cryostat of $5{\cdot}10^{-7}$ mbar, the TEC device presented in section 1 enables to reach an operating temperature of 184 K on the long term.

B. Linearity

To assess detector linearity, a 2-μm laser diode Nanoplus has been used in combination with a wheel of calibrated densities. The laser diode is set up in front of the quartz window of the detector and illuminates widely the APD. Densities are added between the quartz window and the laser diode to provide a large set of transmittances (see figure 5).

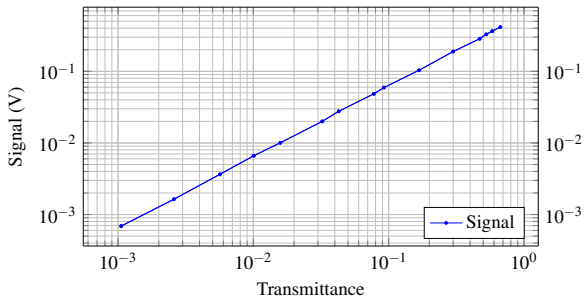

Figure 5: Signal intensity versus transmittance at 2 μm. Transmittance is accurately known thanks to FTIR calibrated values of the optical densities. Laser intensity drift is taken into account to correct the signal. Reverse bias is set to 12V and operating temperature is 185 K.

The incident power with transmittance $T = 1$ was roughly 2 μW. Hence the detector was proved to achieve close to linear reponse over 3 orders of magnitude (from nW to μW). The experimental setup shows a root mean square error of 1,8 % from ideal linear response.

C. Gain and NEP as a function of revers bias

We confront here the numerical prediction presented in first section with experimental data (see figure 6).

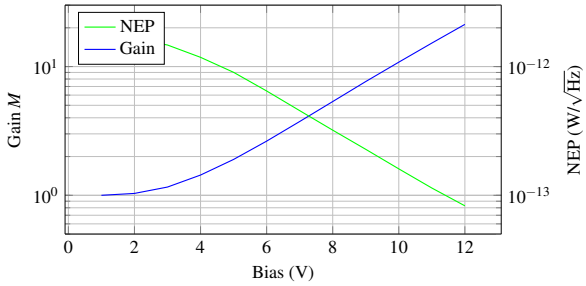

Figure 6: Experimental gain and NEP records as a function of reverse bias. Operating temperature is 185K.

For a reverse bias of 12V, a gain of 21 is achieved. Corresponding NEP is about 80 fW/$\sqrt{\text{Hz}}$.

D. Noise

Finally we investigate the noise properties with Allan variance tool (see figure 7). This mathematical tool allows to distinguish between white noise, flicker noise, etc. We use the simple estimator $\text{std}(u,\tau) = \sqrt{\frac{1}{m}\sum_{i=1}^{m}(u_{i+1}-u_i)^2}$ where u_i is the averaged voltage value over the duration τ. The $\tau^{-1/2}$ slope corresponds to white noise.

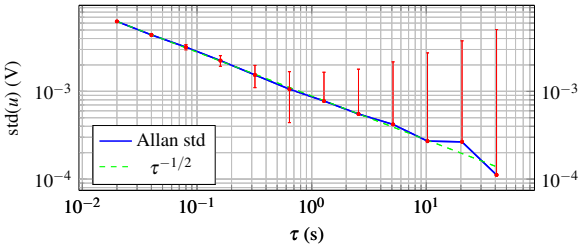

Figure 7: Allan standard deviations computed for a series of 5000 samples with 0,02 s as time step.

Results presented in figure 7 show that there is no evidence of other noises than white noise at the time scale of a few seconds, which was highly suitable to avoid any potential error while averaging over such time gate.

6. CONCLUSION

A HgCdTe APD-based detector for lidar use at 2 μm has been characterized. Key figures of merit are a NEP of 80 fW/$\sqrt{\text{Hz}}$ and a gain of 22 at 12 V reverse bias. At the same reverse bias, spatial response variability is about 2 % and the close to linear dynamic range covers at least three orders of magnitude. Overall bandwidth is 20,5 MHz.

AKNOWLEDGMENTS

The authors thank the french national space agency CNES for supporting this work.

REFERENCES

[1] F. Gibert, D. Edouart, C. Cenac, and F. L. Mounier, ``2-μm high-power multiple-frequency single-mode Q-switched Ho:YLF laser for DIAL application," *Applied Physics B*, 2014.

[2] B. Saleh and M. Teich, *Fundamentals of photonics, p645*. Wiley series, 1991.

[3] J. Beck, T. Welsch, P. Mitra, K. Reiff, X. Sun, and J. Abshire, ``A Highly Sensitive Multi-element HgCdTe e-APD Detector for IPDA Lidar Applications," *Journal of Electronic Materials*, 2014.

[4] K. Foubert, G. Lasfargues, L.Mathieu, and S. Benahmed, ``Developement of hgcdte single-element apds based detectors for low flux short wave infrared applications," *Proceedings SPIE*, 2013.